

Brueckner-Hartree-Fock–based optical potential for proton-^{4,6,8}He and proton-^{6,7,9,11}Li scatteringSyed Rafi,¹ A. Bhagwat,² W. Haider,¹ and Y. K. Gambhir³¹*Department of Physics, Aligarh Muslim University, Aligarh 202 002, India*²*UM-DAE Centre for Excellence in Basic Sciences, Mumbai 400 098, India*³*Manipal University, Manipal 576104, India, and Department of Physics, I.I.T. Powai, Mumbai 400 076, India*

(Received 19 June 2012; revised manuscript received 19 August 2012; published 21 September 2012)

Proton-nucleus scattering provides a useful tool to determine either the parameters entering in the assumed shape of the neutron distribution or to test the reliability of the theoretically calculated neutron distributions in the target nuclei. We have used the Bethe-Brueckner-Hartree-Fock approach to calculate the optical potential for analyzing the experimental observables (e.g., differential cross section and polarization) for p -^{4,6,8}He and p -^{6,7,9,11}Li scattering. The calculation requires mainly two inputs: (1) the nucleon-nucleon (NN) interaction and (2) the nucleon distributions in target nuclei. Various local realistic internucleon (NN) potentials such as Reid93, Urbana v-14, and Argonne v-18 along with several model nucleon density distributions are employed in generating the nucleon-nucleus optical potential. We study the sensitivity of the calculated physical observables on the NN interaction and the density distributions used. It is observed that all the NN interactions and also the different density distributions reproduce rather well the experimental differential cross sections while the calculated polarization is more sensitive to the NN interaction and also to the density distribution used. Thus the polarization data can be used as an additional constraint on the determination of nucleon (especially neutron) density distributions in nuclei. Some results of the representative cases highlighting these features are presented and discussed in detail for illustration.

DOI: [10.1103/PhysRevC.86.034612](https://doi.org/10.1103/PhysRevC.86.034612)

PACS number(s): 24.10.Ht, 21.10.Gv, 21.30.Fe, 25.40.Cm

I. INTRODUCTION

Knowledge of the nucleon distributions in nuclei is of fundamental importance. The neutron distribution in nuclei can be obtained only indirectly, in contrast to the corresponding proton distribution which can be reliably determined through electron scattering. Proton-nucleus scattering provides a useful tool to determine either the parameters entering in the assumed shape of the neutron distribution or to test the reliability of the theoretically calculated neutron distribution. The calculations employ a microscopic complex optical potential generated within the Bethe-Brueckner-Hartree-Fock (BHF) formalism. This g -matrix folding procedure has been and is still being used quite successfully to extract the neutron distributions in several nuclei and also in a variety of isotopic chains of nuclei (for example, see [1]). The method has also been used [2] to extract the parameters appearing in the assumed neutron distributions or to validate theoretically calculated neutron distributions in neutron-rich, loosely bound nuclei by reproducing their available experimental differential cross sections (see, for example, [3]). Further, the method has been used to study neutron-rich exotic nuclei having possible halo structures, such as ^{6,8}He, ¹¹Li [4], and ²²C [5]. Due to their unstable (short-lived) nature, only recently have the experimental polarization (A_y) data in p - A scattering involving these exotic nuclei started to appear. These experiments needed to be performed in inverse kinematics. For example, the elastic scattering of radioactive ions from hydrogen [6] in inverse kinematics corresponds to proton scattering from the heavy ions. Very recently, the analyzing power or polarization (A_y) for p -⁶He scattering at 71 MeV/nucleon has been reported [7]. Uesaka *et al.* [7] have used the Bonn B potential in the Brueckner-Hartree-Fock approach along with single-particle densities obtained by employing a harmonic oscillator and

also a Woods-Saxon potential to generate the required optical potential for analyzing the experimental data. The differential cross section is reasonably well reproduced at forward angles. On the other hand, the analyzing power does not seem to be compatible with the g -matrix folding model predictions, indicating its sensitivity to the model used for the nuclear structure. It should be pointed out that the reported analyzing power data have substantial errors and therefore the need for more accurate measurements is stressed.

Helium isotopes offer a unique and very interesting example for accurate microscopic theoretical studies. ⁴He is the lightest doubly magic nucleus, ⁶He is expected to have a neutron halo akin to that of the celebrated ¹¹Li, and ⁸He is supposed to have a thick neutron skin. We present here systematic analysis of p -^{4,6,8}He and p -^{6,7,9,11}Li scattering data using a BHF-based optical potential. Relativistic kinematics is used, which necessitates a recalculation of the self-consistent nucleon-nuclear matter optical potential. The spin-orbit part of the potential is calculated by carefully avoiding the short-range approximation [8]. We use an effective mass correction [9], leading to a modification of the real and imaginary parts of both the central and spin-orbit components of the optical potential. The resulting optical potential is complex and is energy and density dependent (for details see Ref. [10]). We employ local realistic internucleon (NN) potentials—Urbana v-14 [11], Argonne v-18 [12], and Reid93 [13]—along with several model nucleon density distributions required in generating the nucleon-nucleus optical potential to study the sensitivity of the calculated observables such as the differential cross sections and polarization on the NN interactions and the nucleon density distributions used. It is found that all the NN interactions and different density distributions satisfactorily reproduce the experimental differential cross sections whereas the calculated polarization is more sensitive to the

NN interaction as well as to the density distribution used. Thus the polarization data impose an additional constraint on the determination of nucleon (especially neutron) density distributions in nuclei. The experimental analyzing power data presently available have substantial errors and therefore more accurate and additional polarization data are needed to extract reliable nucleon (neutron) density distributions in these loosely bound neutron-rich nuclei.

Section II presents briefly the method of calculating the optical potential. The results are presented and discussed in Sec. III. The main conclusions are contained in Sec. IV.

II. METHOD OF CALCULATION

A. Optical potential

In order to calculate the microscopic nucleon optical potential for finite nuclei in Brueckner theory, one essentially requires two inputs: the realistic NN interaction to calculate the reaction matrices and point-nucleon density distributions to be used for folding the reaction matrices using the local density approximation (LDA) [14,15]. We solve the Bethe-Goldstone integral equation to obtain reaction matrices using three modern local soft-core Urbana *v*-14 [11], Argonne *v*-18 [12], and Reid93 [13] internucleon potentials. We use relativistic kinematics for calculating the momentum of both the incident and target nucleons in calculating the effective interaction.

Self-consistency is achieved in about five cycles for each of the 17 nuclear matter densities spread evenly over the range of Fermi momentum $k_F = 0.6\text{--}2.0\text{ fm}^{-1}$, in the incident momentum region $0.1\text{--}8.0\text{ fm}^{-1}$. The self-consistent BHF calculations have been performed for nuclear matter at a large number of densities. We fold the appropriate numerically computed complex reaction matrices (as defined in Ref. [10]) over the proton- and neutron- density distributions (Sec. II B) using the LDA to obtain both central and spin-orbit parts of the potential. In view of the importance of spin effects, we avoid the normally used [16] short-range approximation and calculate the folding integral for the direct part of the spin-orbit potential without any approximation [8]. Such a reaction matrix approach has been successfully applied in the past (see, for example, Refs. [4,7,10,17]).

The numerically calculated energy- and density-dependent complex reaction matrices are folded [18,19] over the nucleon density distributions in the nucleus to obtain the microscopic nucleon-nucleus real (imaginary) parts of the central $V(E, r)$ ($W(E, r)$) and the spin-orbit $V_{SO}(E, r)$ ($W_{SO}(E, r)$) components of the optical potential.

In order to obtain agreement with the experimental data, following normal practice, we multiply each component of the calculated potential by scaling parameters λ . The potential ($U(E, r)$) used to calculate observables in a spherical optical model code is

$$U(E, r) = \lambda_R V(E, r) + i\lambda_I W(E, r) + \lambda_{SO}^R V_{SO}(E, r) + i\lambda_{SO}^I W_{SO}(E, r). \quad (1)$$

Thus, in principle, there are four adjustable (scaling) parameters (λ_R , λ_I , λ_{SO}^R , and λ_{SO}^I) to obtain a best fit to the

experimental data by minimizing χ^2/DF (where DF stands for degrees of freedom).

In practical calculations, only a few (or no) scaling parameters are used. In particular, for ${}^4\text{He}$, the agreement with the experiment for the differential cross section and polarization remains almost unchanged, with or without scaling parameters (i.e. all λ 's are unity). For the case of ${}^6,8\text{He}$ and ${}^{7,9,11}\text{Li}$, the agreement with the experiment is improved with the optimal value of $\lambda_I = 0.7$ and keeping all the remaining λ 's fixed to unity. However, for ${}^6\text{Li}$, it is found that $\lambda_I = 1.2$ and $\lambda_R = 0.7$ are required to obtain the improved fit to the experiment.

In the present work, three-body terms of the nucleon-nucleon forces have been neglected. In fact, it has recently been shown [20] that the effect of the three-body force on the microscopically calculated potential is to reduce the strengths of the central part of the optical potential in the nuclear interior only. The effect on the spin-orbit potential is nearly insignificant. This results in a slight improvement in the agreement with the experiment for the polarization for $p\text{-}{}^{12}\text{C}$, $p\text{-}{}^{40}\text{Ca}$, $p\text{-}{}^{90}\text{Zr}$, and $p\text{-}{}^{208}\text{Pb}$ scattering, while the agreement for the differential cross sections is almost unaffected. Hence we do not expect substantial change in the proton scattering observables at the low energies considered in the present work. Our preliminary results concerning the effect of three-body forces confirm this conjecture. A detailed investigation dealing with the effects of the three-body force on the calculated optical potential is in progress.

B. Semiphenomenological densities

It is well known that the shell model or other mean-field calculations do not make allowance directly for very low binding energies of the valance nucleons (neutrons). Therefore, these calculations do not necessarily yield the correct description of loosely bound nuclei. It is therefore a common practice to use in the reaction calculations the semi-empirical or model nucleon density distributions that take the effects like ‘‘halo’’ and ‘‘skin’’ into account. The density that has also been employed in the present work has been used successfully in the past to describe the reaction cross sections of loosely bound nuclei (see Refs. [5,21]).

A semiphenomenological model for nucleon density distributions within a nucleus with Z protons and N neutrons has been proposed in the literature [22]. The model satisfies two important physical requirements, namely, the correct behavior near the center ($r \rightarrow 0$) and the right asymptotic behavior ($r \rightarrow \infty$). The former implies that the power series expansion of the density near the origin will have only even powers of r , whereas the latter means that, asymptotically, the density should behave as

$$\rho_i(r) \rightarrow r_i^{-2\alpha_i} e^{-r/a_i}, \quad (2)$$

with

$$a_i = \frac{\hbar}{\sqrt{8m\epsilon_i}} \quad (3)$$

and

$$\alpha_i = q\alpha_f \sqrt{\frac{mc^2}{2\epsilon_i}} + 1. \quad (4)$$

Here, α_f is the fine-structure constant; $i = n$ or p ; $q = Z - 1$ for protons and 0 for neutrons; ϵ_i is the corresponding nucleon separation energy; and m is the reduced mass, which, for simplicity, is taken to be the nucleon mass. The following simple expression fulfilling the above requirements was proposed [22]:

$$\rho_i(r) = \frac{\rho_i^0}{1 + \left[\frac{(1+(r/R)^2)}{2} \right]^{\alpha_i} [e^{(r-R)/a_i} + e^{-(r+R)/a_i}]} \quad (5)$$

Here, the normalization constants ρ_n^0 and ρ_p^0 have been determined from the requirements

$$4\pi \int \rho_n r^2 dr = N, \quad (6)$$

$$4\pi \int \rho_p r^2 dr = Z. \quad (7)$$

The only parameter that is unknown here is R (the radius parameter), which is determined by reproducing the experimentally measured rms radius of charge density. The same radius parameter is used in the neutron densities as well.

The loosely bound nuclei, having neutron/proton excess, evidently, have a small separation energy and hence a prominent tail in the corresponding density profile. For such systems, the ‘‘core’’ (tightly bound) and ‘‘tail’’ (loosely bound) parts should be treated adequately. For example, let N , Z be the neutron and proton numbers of the neutron-rich nucleus. Let N_c , Z_c be the neutron and proton numbers of the core. For neutron-rich nuclei we take $Z_c = Z$. Then, according to the model discussed in [21], the neutron density distribution for the nucleus (N , Z) is written as

$$\rho_n(N, Z; r) = \rho_{\text{core}}(N_c, Z; r) + \rho_{\text{tail}}(N - N_c; r).$$

Here, the core part of the density is given by Eq. (5), with separation energy corresponding to the core nucleus. For the tail part, which is normalized to $N - N_c$, we use [21]

$$\rho_{\text{tail}} = N_0 \left(\frac{r^2}{(r^2 + R^2)^2} \right) e^{-r/a_t}, \quad (8)$$

with N_0 being a normalization constant and a_t as defined above in Eq. (3) with separation energy corresponding to the loosely bound nucleus. By assuming that the experimental charge radius of the nucleus (N , Z) is known, the parameter R in the core as well as in the tail part is taken to be the same as that for the actual nucleus. In a loosely bound nucleus, the core density is taken as it is, and in the tail part, the R parameter from the actual nucleus is used. The proton densities correspond to those obtained by using the actual experimental charge radii. In this model, the neutron densities of ${}^6, {}^8\text{He}$ and ${}^8, {}^9, {}^{11}\text{Li}$ are expressed as [21]

$$\rho_n({}^6\text{He}; r) = \rho_n(N = 2, Z = 2; r) + \rho_n(2; r),$$

$$\rho_n({}^8\text{He}; r) = \rho_n(N = 2, Z = 2; r) + \rho_n(4; r),$$

$$\rho_n({}^8\text{Li}; r) = \rho_n(N = 4, Z = 3; r) + \rho_n(1; r),$$

$$\rho_n({}^9\text{Li}; r) = \rho_n(N = 4, Z = 3; r) + \rho_n(2; r),$$

$$\rho_n({}^{11}\text{Li}; r) = \rho_n({}^9\text{Li}; r) + \rho_n(2; r).$$

TABLE I. The calculated neutron (r_n), proton (r_p), and matter radii (r_m), using R fixed by reproducing experimental charge radii (r_c). The matter radii obtained reported earlier have also been included for comparison.

	R (fm)	r_n (fm)	r_p (fm)	r_m (fm)	r_c (fm)
${}^4\text{He}$	0.892	1.469	1.472	1.471	1.675 ^a
		1.473	1.473	1.473	1.676 ^b
		1.425	1.425	1.425	1.634 ^c
${}^6\text{He}$	1.668	3.205	1.907	2.839	2.067
				2.586 ^d	
				2.54 ^e	
${}^8\text{He}$	1.490	3.069	1.755	2.799	1.928
				2.946 ^d	
				2.60 ^f	
${}^6\text{Li}$	1.028	2.359	2.387	2.373	2.550
${}^7\text{Li}$	1.582	2.526	2.252	2.412	2.402
${}^8\text{Li}$	1.626	2.854	2.155	2.614	2.295
				2.516	2.199
${}^9\text{Li}$	1.582	2.713	2.068	2.579 ^d	
				2.30 ^e	
${}^{11}\text{Li}$	2.072	3.677	2.334	3.364	2.434
				2.964 ^d	
				3.53 ^e	

^aReference [23].

^bReference [30].

^cReference [31].

^dReference [4].

^eReferences [24,25].

^fReference [32].

The calculated neutron (r_n), proton ($r_p = \sqrt{r_c^2 - 0.64}$), and matter [$r_m = (Zr_p + Nr_n)/(Z + N)$] radii along with the corresponding charge radii (r_c) are listed in Table I. The charge radii used in the present work have been adopted from [23]. The r_m values obtained by Karataglidis *et al.* [4], from the Glauber model analysis [24,25], as well as from a few-body analysis (for ${}^8\text{He}$) have also been presented for comparison. It should be noted that the values of radii of the phenomenological density reported here differ slightly from those reported in [21], primarily due to the fact that the charge radii of these isotopes were unknown at that time. It is only recently that they have been reported in the literature [26–29]. Due to the presence of loosely bound nucleons, the charge radii of these nuclei turn out to be larger than what was expected earlier from the Glauber model analysis (see the discussion in Ref. [21]). In the case of ${}^4\text{He}$, we use the density obtained by unfolding the experimental [sum of Gaussians (SOG)] charge density [30]. In addition, the point-proton density distribution reported by McCarthy *et al.* [31] has also been used.

III. RESULTS AND DISCUSSION

We now present and discuss the results of p - ${}^4, {}^6, {}^8\text{He}$ scattering followed by that of p - ${}^6, {}^7, {}^9, {}^{11}\text{Li}$ scattering.

A. He isotopes

The nuclei in this region involve a small number of nucleons and therefore basic and fundamental accurate theoretical calculations are feasible. In fact, several sophisticated calculations have been reported for He isotopes (specially for ${}^4\text{He}$) in which techniques such as Green's function Monte Carlo [33], the resonating group method [34], the microscopic multicluster model [35], Fadeev-Yakubovsky four-body equations [36], hyperspherical functions [37], and the *ab initio* shell model have been employed.

1. ${}^4\text{He}$

${}^4\text{He}$ is quite unique; it is the lightest doubly magic and most tightly bound nucleus. The most sophisticated calculations for ${}^4\text{He}$ predict that the point-proton density in the extreme interior is around 0.2 proton/ fm^3 or more, which is much larger than the commonly expected value. It is interesting to point out that in spite of the available accurate descriptions of the ${}^4\text{He}$ nucleus its calculated density distributions have seldom been used in the analysis of p - ${}^4\text{He}$ scattering where the experimental data for both differential cross section and the polarization exist.

For ${}^4\text{He}$ we have calculated the point-proton density distribution by unfolding the experimental charge distribution resulting from a model-independent analysis of the electron scattering data in terms of a SOG [30]. The neutron density distribution is assumed to be the same as the proton distribution. Two such sets [30] and [31] labeled as unfolded and McCarthy *et al.*, respectively, are shown in Fig. 1. The same results are also plotted in the inset on a semilog scale. It is seen that the two densities are almost similar as expected, except at small distances (0.5 to 1.0 fermi). The rise (peak) around 0.8 fm is due to the unfolding of the experimental SOG density.

The calculated differential cross section ($d\sigma/d\Omega$) for a 71.9-MeV proton incident on a ${}^4\text{He}$ target, calculated using Reid93, Urbana v-14, and Argonne v-18 realistic internucleon (NN) potentials along with the unfolded density distribution is displayed in Fig. 2. All three interactions yield more or less the

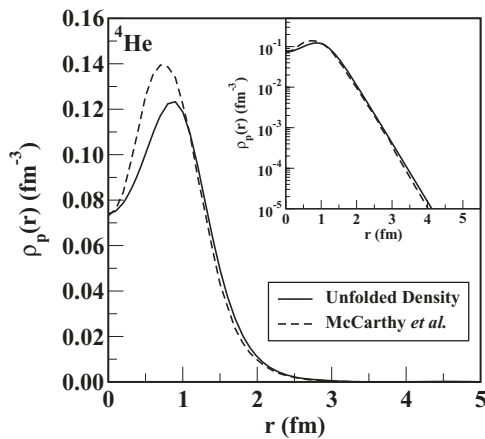


FIG. 1. Extracted (unfolded) point-proton density distribution in ${}^4\text{He}$. The charge densities have been taken from [30]. The corresponding densities, reported by McCarthy *et al.* [31] are also presented for comparison. The same results are plotted in the inset on a semilog scale.

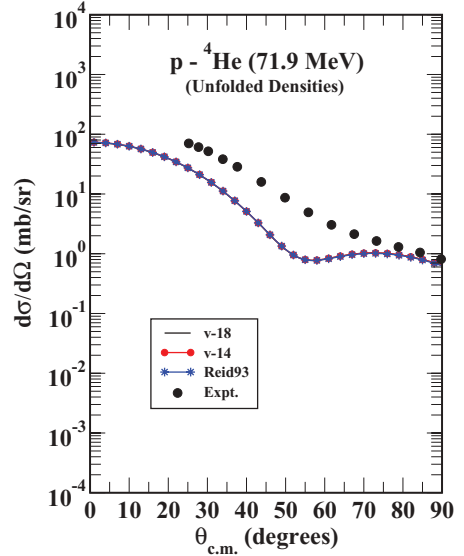


FIG. 2. (Color online) The calculated differential cross section for 71.9-MeV p - ${}^4\text{He}$ scattering obtained by using different NN interactions: v-18, v-14, and Reid93. The unfolded densities, as described in the text, have been used. The corresponding experimental values, taken from [38], are also shown for comparison. Here, all three interactions (v-18, v-14, and Reid93) yield almost the same results. Therefore the corresponding curves almost coincide.

same results. Therefore, the respective curves almost coincide. Thus, it is difficult to distinguish the curves individually in the figure. Further, the corresponding results obtained by using the second set [31] of the density distribution is expected to be very similar (see Fig. 3). Clearly, the calculation somewhat

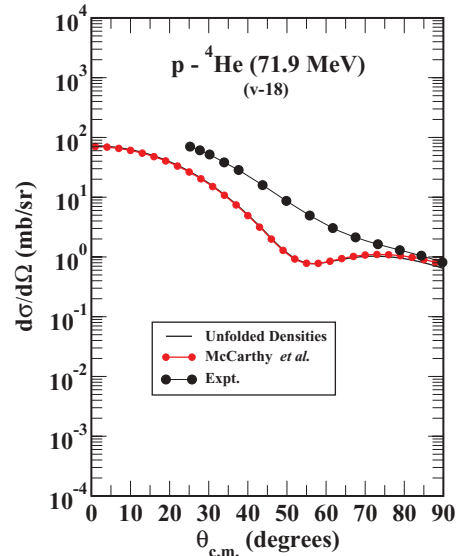


FIG. 3. (Color online) The calculated differential cross section for 71.9-MeV p - ${}^4\text{He}$ scattering obtained by using different density distributions: unfolded and that reported by McCarthy *et al.* [31]. The Argonne v-18 interaction has been employed. The experimental data, also shown, have been taken from [38]. Here, the results obtained by using the two densities are almost identical. Therefore the corresponding curves almost coincide.

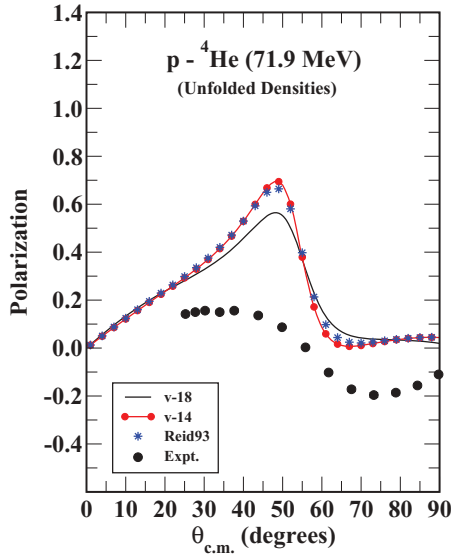


FIG. 4. (Color online) The calculated polarization (A_y) for 71.9-MeV p - ^4He scattering obtained by using different NN interactions: v-18, v-14, and Reid93. The unfolded densities, as described in the text, have been used.

underestimates the experimental differential cross sections [38] at lower angles up to $\theta_{cm} \sim 70^\circ$. Figure 3 shows similar results obtained by using both sets of density distributions and the v-18 NN potential. Clearly, the two density distributions yield almost identical results; hence, the respective curves coincide, making it difficult to distinguish them from each other. However, it is found that the two calculations differ from the corresponding experiment as observed in Fig. 3. Similar results for polarization (A_y) are displayed in Figs. 4 and 5, respectively, along with the corresponding experimental

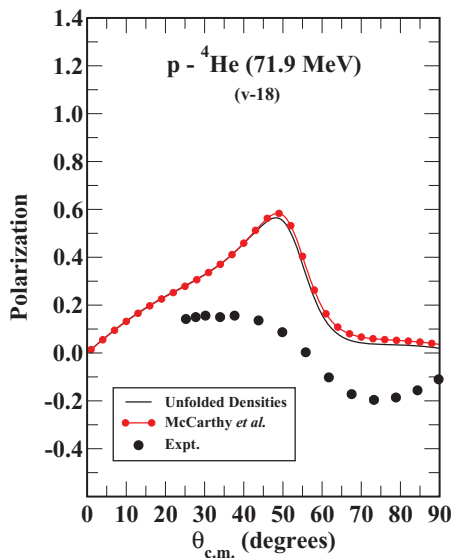


FIG. 5. (Color online) The calculated polarization (A_y) for 71.9-MeV p - ^4He scattering obtained by using different density distributions: unfolded and that reported by McCarthy *et al.* [31]. The Argonne v-18 interaction has been employed.

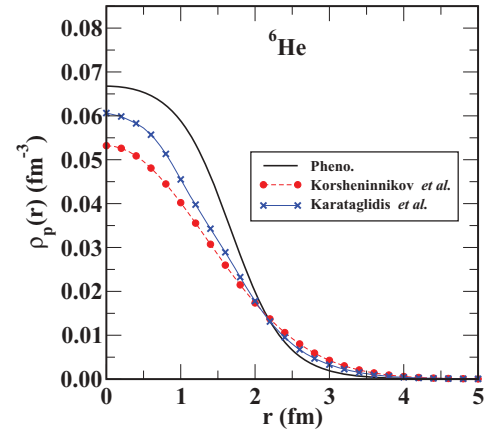


FIG. 6. (Color online) Point-proton density distribution in ^6He : Pheno [21], Karataglidis *et al.* [4], and Korshennikov *et al.* [6].

data taken from Ref. [38]. Both the calculated (varying between 0.0 and ~ 0.6) and the experimental (varying between 0.1 and -0.2) polarization ranges have small magnitudes. The calculated results somewhat overestimate the experiment though both exhibit similar trends. Figure 4 indicates that the results obtained with an unfolded density distribution and using Reid93 and Urbana v-14 NN interactions are identical while that of Argonne v-18 are somewhat smaller and therefore are closer to the experiment. Figure 5 clearly shows that the results obtained with the v-18 interaction and using both sets of density distributions are almost identical as anticipated and slightly overestimate the experiment. It is observed that the calculated results for ^4He deviate the most from the corresponding experimental values. Such a strong deviation may be attributed to the inadequacy of the LDA for such a light nucleus.

2. ^6He

Recently, Uesaka *et al.* [7] reported analyzing power A_y (polarization) data for p - ^6He elastic scattering at

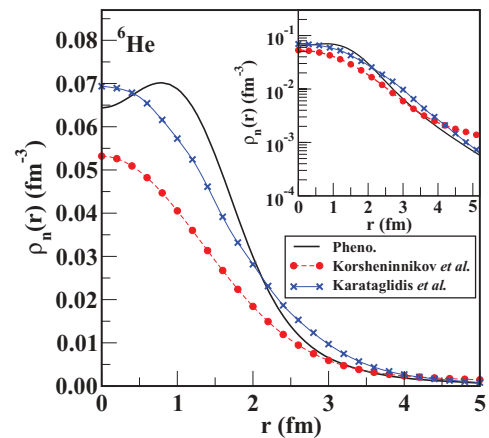


FIG. 7. (Color online) Neutron density distribution in ^6He : Pheno [21], Karataglidis *et al.* [4] and Korshennikov *et al.* [6]. The same results are plotted in the inset on a semilog scale.

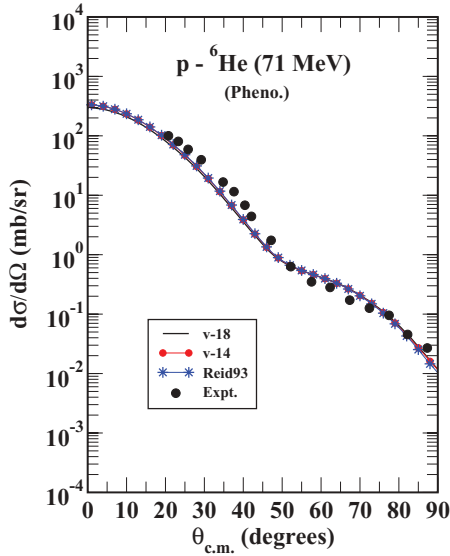


FIG. 8. (Color online) The calculated differential cross section for p - ${}^6\text{He}$ (71 A MeV) scattering obtained by using v -18, v -14, and Reid93 NN interactions, with semi-empirical (Pheno) nucleon density distributions. The corresponding experimental values [7] of the differential cross sections are also presented for comparison.

71 MeV/nucleon using a polarized proton target. The authors analyzed both the differential cross section ($d\sigma/d\Omega$) and the A_y data within the g -matrix folding model using the Bonn B NN potential along with single-particle wave functions generated using a Woods-Saxon (WS) potential with and without a halo component. Earlier, Karataglidis *et al.* [4] (Korshennikov *et al.* [6]) analyzed ($d\sigma/d\Omega$) data for p - ${}^6\text{He}$ elastic scattering at 72 A MeV (70 A MeV). The former

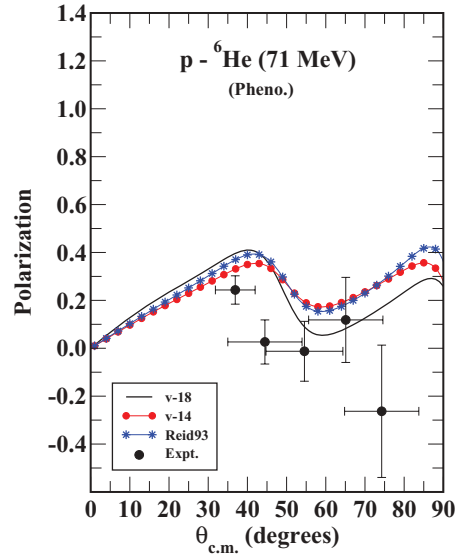


FIG. 10. (Color online) The calculated polarization (A_y) for p - ${}^6\text{He}$ (71 A MeV) scattering obtained by using v -18, v -14, and Reid93 NN interactions, with semi-empirical (Pheno) nucleon density distribution. The corresponding experimental values [7] of the differential cross sections are also presented for comparison.

authors [4] employed the g -matrix folding model using the Reid93 NN potential together with an *ab initio* shell model and its variant for calculating the density distributions with and without a halo component. The latter authors [6] carried out optical model calculations within the eikonal approximation and the density distribution obtained using the cluster-orbital shell model ($\alpha + 2n$ model for ${}^6\text{He}$) approximation (COSMA) [39]. We have used in our calculations local Reid93, v -14,

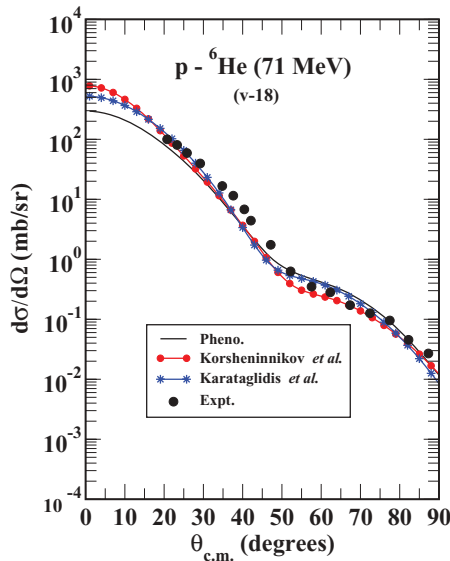


FIG. 9. (Color online) The calculated differential cross section for p - ${}^6\text{He}$ (71 A MeV) scattering obtained by using nucleon density distributions of Pheno [21], Karataglidis *et al.* [4], and Korshennikov *et al.* [6]. The corresponding experimental data [7] are also shown for comparison.

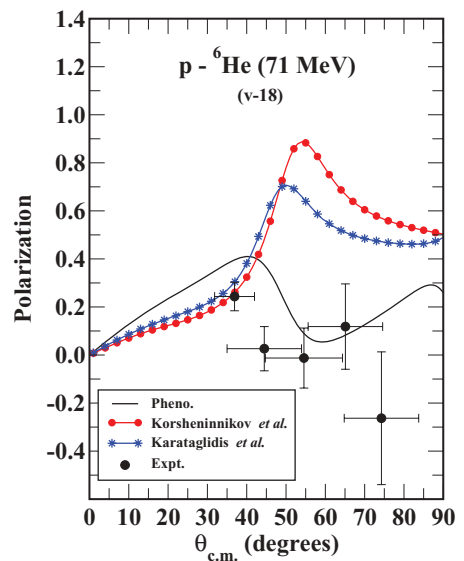


FIG. 11. (Color online) The calculated polarization (A_y) for p - ${}^6\text{He}$ (71 A MeV) scattering obtained by using nucleon density distributions of Pheno (ours), Karataglidis *et al.* [4], and Korshennikov *et al.* [6]. The corresponding experimental data [7] are also shown for comparison.

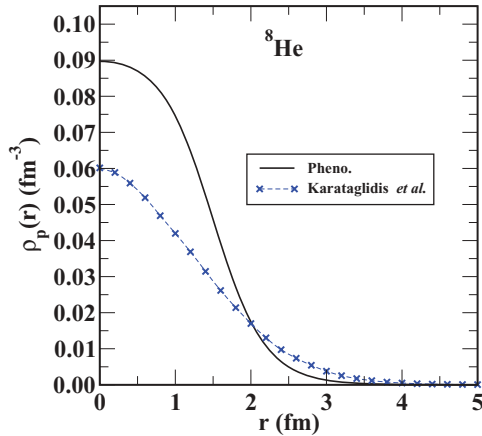


FIG. 12. (Color online) Point-proton density distribution in ${}^8\text{He}$: Pheno [21] and Karataglidis *et al.* [4].

and v-18 NN potentials and the density distributions of both Korshennikov *et al.* [6] and of Karataglidis *et al.* [4] with a halo component. In addition we have also employed semi-empirical density distributions proposed and successfully applied by some of us [5,21,22] for the description of loosely bound nuclei. The proton and the neutron density distributions used are presented in Figs. 6 and 7, respectively. The neutron densities have also been plotted in the inset of Fig. 7 on a semilog scale to demonstrate the possible halo structure. These density distributions (Pheno and those reported in Refs. [4,6]) substantially differ from each other at small r , for protons as well as for neutrons. All three calculations (Pheno and those reported in Refs. [4,6]), as seen from Fig. 7, indicate halo structure for the neutron density distribution as expected.

The calculated $d\sigma/d\Omega$ for 71 A MeV p - ${}^6\text{He}$ scattering is displayed in Fig. 8 obtained by using the Pheno density distribution and all the three: v-18, v-14, and Reid93 interactions. Similar results obtained by using the v-18 interaction, and all three nucleon density distributions are displayed in Fig. 9. Figures 8 and 9 clearly indicate that all three interactions and all three density distributions considered here, though different,

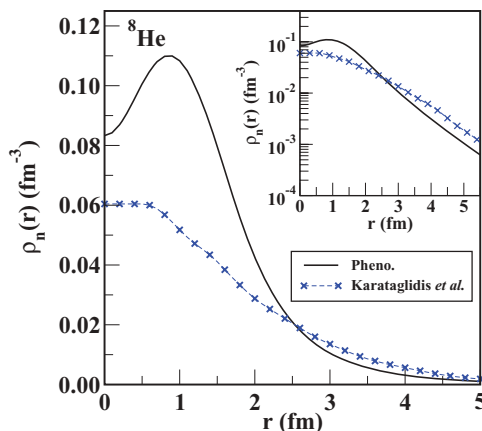


FIG. 13. (Color online) Neutron density distribution in ${}^8\text{He}$: Pheno [21] and Karataglidis *et al.* [4]. The same results are plotted in the inset on a semilog scale.

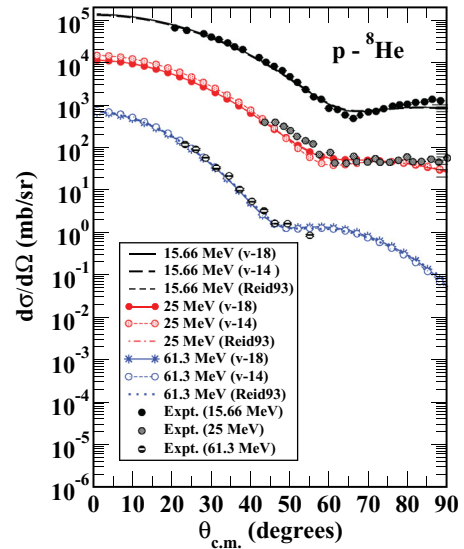


FIG. 14. (Color online) The calculated differential cross section for p - ${}^8\text{He}$ scattering at different energies (15.66, 25, and 61.3 A MeV) obtained by using v-18, v-14, and Reid93 NN interactions. The semi-empirical (Pheno) nucleon density distribution is used. The data at 25 MeV (15.66 MeV) are multiplied by a scaling factor of 10 (100).

reproduce the experiment rather well. The quality of agreement is nearly the same in all cases.

Corresponding results for the polarization are presented in Figs. 10 and 11, respectively. It can be seen from Fig. 10 that the calculation using all three interactions along with the Pheno density distribution qualitatively reproduces the experimental trend but does deviate in magnitude, and the results with the v-18 interaction are the closest to the experiment. On the other hand, the v-18 results presented in Fig. 11 indicate that the

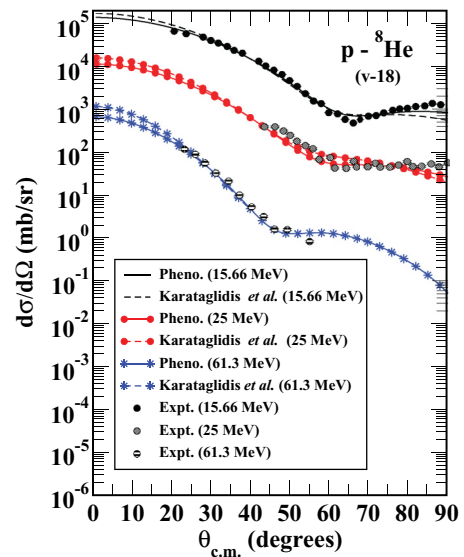


FIG. 15. (Color online) The calculated differential cross section for p - ${}^8\text{He}$ scattering at different energies (15.66, 25, and 61.3 A MeV) obtained by using nucleon density distributions of Figs. 12 and 13. The data at 25 MeV (15.66 MeV) are multiplied by a scaling factor of 10 (100).

use of different density distributions leads to different results, which deviate from the experiment. The results with the Pheno density distribution are closest and qualitatively reproduce the experiment. This observation implies that the polarization data are indeed sensitive and introduces an additional constraint to the nucleon density distribution used in the calculation. However, it is important to note that the present polarization data are few and also have large experimental errors. Hence, to determine reliably the nucleon density distribution (specially of neutrons) one needs additional and accurate experimental polarization data, which hopefully, will be available in the near future.

3. ${}^8\text{He}$

Recently, Mackintosh and Keeley [17] reported differential cross section data for p - ${}^8\text{He}$ scattering at three different energies: 15.66, 25, and 61.3 A MeV. Therefore, to investigate the energy dependence we have repeated the calculation for p - ${}^8\text{He}$ scattering at all three energies. All three (v-18, v-14, and Reid93) NN interactions along with two (Pheno [21] and that of Karataglidis *et al.* [4] with a halo component) nucleon density distributions have been used to calculate the corresponding optical potentials. These density distributions are shown in Figs. 12 and 13 for protons and neutrons, respectively. The neutron densities have also been plotted in the inset of Fig. 13 on a semilog scale to emphasize the extended neutron density distribution. It is found that the two density distributions (Pheno and that reported by Karataglidis *et al.* [4]) are clearly different at small r as well as at large r , for protons as well as for neutrons. Neutron distributions indicate thick neutron skin, which is absent in the corresponding proton distributions. The calculated differential cross sections ($d\sigma/d\Omega$) with the Pheno density distribution for all three energies are shown in Fig. 14

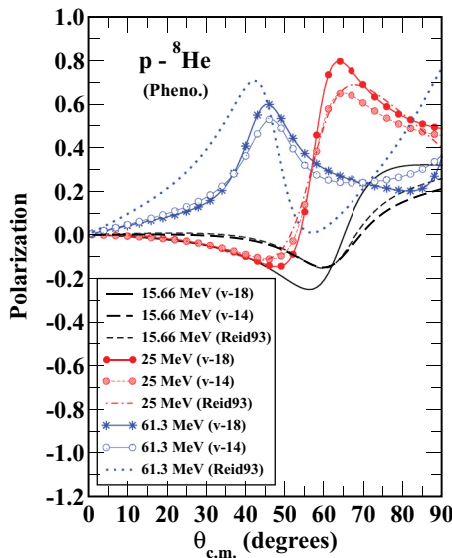


FIG. 16. (Color online) The calculated polarization (A_y) for p - ${}^8\text{He}$ at different energies (15.66, 25, and 61.3 A MeV) obtained by using v-18, v-14, and Reid93 NN interactions. The semi-empirical (Pheno) nucleon density distributions are used in the calculation.

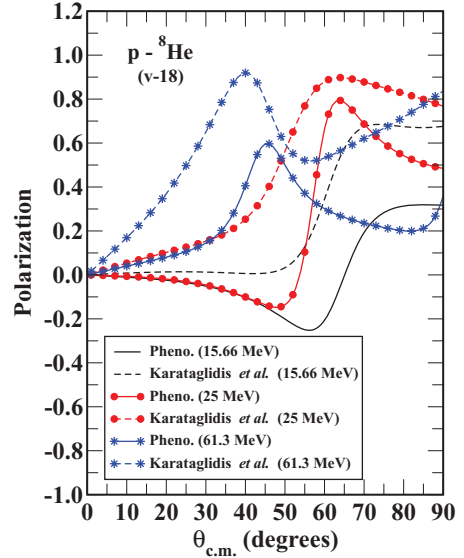


FIG. 17. (Color online) The calculated polarization (A_y) for p - ${}^8\text{He}$ at different energies (15.66 and 61.3 A MeV) obtained by using nucleon density distributions of Figs. 12 and 13. The NN interaction employed here is v-18.

for all three interactions and in Fig. 15 for the v-18 interaction and both density distributions (Figs. 12 and 13).

We note that all the interactions with the Pheno density distribution yield almost identical results and reproduce the experiment rather well at all three energies as expected. Further, the two [4,21] sets of density distributions yield almost identical results, which are very close to the experiment at all three energies (see Fig. 15). The corresponding calculated results for polarization are displayed in Figs. 16 and 17, respectively. The figures show that all the interactions give almost similar results at each energy. Different interactions yield slightly different magnitudes of the first maxima and its position shifts toward smaller angles with increase in energy. Further, the results presented in Fig. 17 are found to be more sensitive to the density distribution used. The two sets of density distributions give almost similar shapes at all energies,

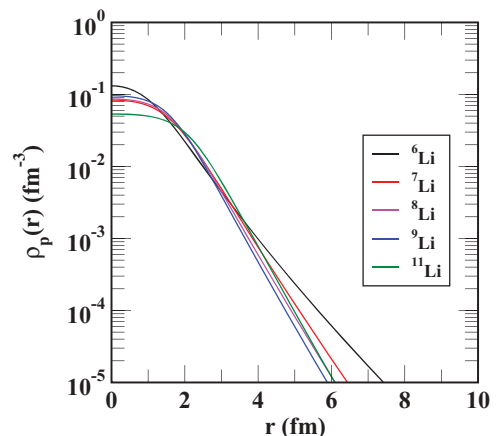


FIG. 18. (Color online) Semiphenomenological (Pheno) point-proton density distributions in ${}^6,7,8,9,11\text{Li}$.

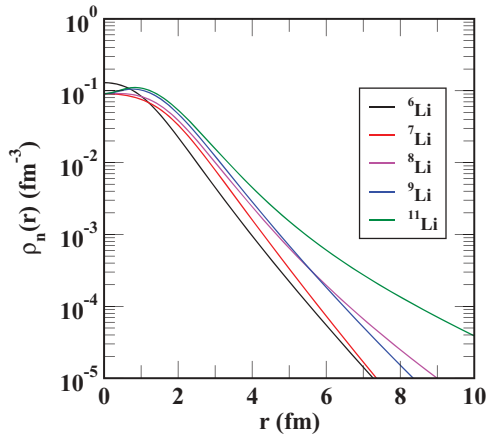


FIG. 19. (Color online) Semiphenomenological (Pheno) point-neutron density distributions in ${}^6,7,8,9,11\text{Li}$.

though the magnitude of the first maxima is appreciably different. Unfortunately, no experimental data exist with which to compare the calculation.

B. Li isotopes

The Pheno proton and neutron density distributions used in the calculation for the case of p - ${}^6,7,8,9,11\text{Li}$ are displayed in Figs. 18 and 19, respectively. The neutron halo structure is evident from Fig. 19 for ${}^{11}\text{Li}$ as expected.

The calculated differential cross sections obtained by using v -18, v -14, and Reid93 NN interactions along with the

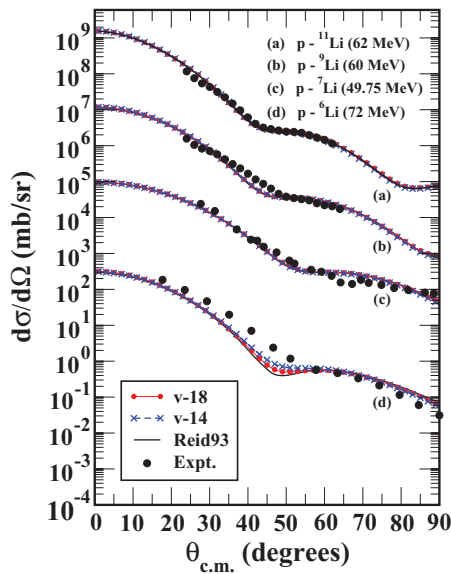


FIG. 20. (Color online) The calculated differential cross section for p -Li scattering obtained by using different NN interactions: Reid93, v -18, v -14, and semiphenomenological (Pheno) nucleon density distributions (Figs. 18 and 19). The data for ${}^7\text{Li}$, ${}^9\text{Li}$, and ${}^{11}\text{Li}$ have been multiplied by scaling factors of 10^2 , 10^4 , and 10^6 , respectively. The experimental data for ${}^6\text{Li}$ and ${}^7\text{Li}$ have been taken from Refs. [40,41], respectively, whereas those for ${}^9\text{Li}$ and ${}^{11}\text{Li}$ have been taken from Ref. [42].

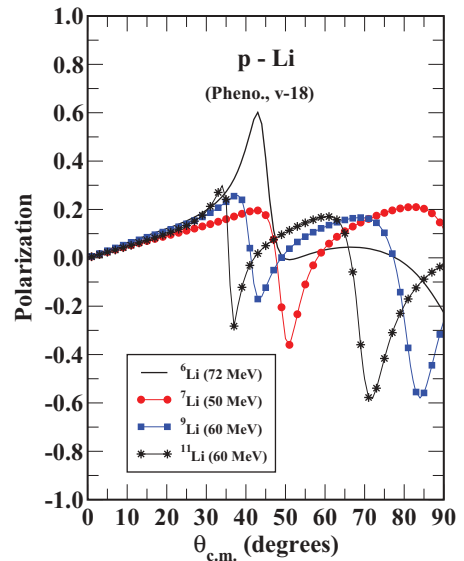


FIG. 21. (Color online) The calculated polarization (A_y) for p -Li scattering using different NN interactions: Reid93, v -18, v -14, and semiphenomenological (Pheno) nucleon density distributions (Figs. 18 and 19).

Pheno nucleon density distributions for p - ${}^6,7,9,11\text{Li}$ scattering are shown in Fig. 20. The corresponding experimental data [40–42] are also shown for comparison. Clearly, all the interactions reproduce the corresponding experiment well. The calculated analyzing power (polarization) is displayed in Fig. 21. It is observed from the figure that ${}^6\text{Li}$ exhibits a stronger (weaker) first maxima (minima), as compared to those of ${}^7,9,11\text{Li}$. Further, the position of the first minima shifts toward smaller angles with increasing mass number. Unfortunately, apart from ${}^6\text{Li}$, no experimental data for polarization exist and therefore no detailed comparison between the calculation and the experiment can be made. Hopefully, our prediction for polarization can be tested when the corresponding experimental data become available in the future.

IV. SUMMARY AND CONCLUSIONS

The Bethe-Brueckner-Hartree-Fock-based optical potential is used in the calculation of experimental observables (e.g., differential cross section and polarization) for p - ${}^4,6,8\text{He}$ and p - ${}^6,7,9,11\text{Li}$ scattering. We have used various local realistic internucleon (NN) potentials such as Reid93, Urbana v -14, and Argonne v -18 along with several model nucleon density distributions required in generating the nucleon optical potential. We study the sensitivity of the calculated physical observables on the NN interaction and the density distributions used. It is observed that all the NN interactions and so also the different density distributions reproduce rather well the experimental differential cross sections while the calculated polarization is found to be more sensitive to the NN interaction and the density distribution used. Thus the polarization data impose an additional constraint on the determination of nucleon (especially neutron) density distributions in nuclei, and therefore they may play an important role in the determination of reliable neutron distributions in nuclei.

ACKNOWLEDGMENTS

Two of us (AB and YKG) wish to acknowledge the Department of Science and Technology (DST), Government of India, for partial financial assistance under Project No. SR/S2/HEP-34/2009. WH gratefully acknowledges a financial

grant from the Department of Atomic Energy (DAE) Board of Research in Nuclear Science (BRNS), Government of India, under BRNS Project No. 2011/37P/16/BRNS. The authors thank Manjari Sharma, Dipti Pachouri, M. Gupta, and S. H. Patil for their interest in this work.

-
- [1] S. Karataglidis, K. Amos, B. A. Brown, and P. K. Deb, *Phys. Rev. C* **65**, 044306 (2002).
- [2] J. Zenihiro *et al.*, *Phys. Rev. C* **82**, 044611 (2010).
- [3] K. Amos, S. Karataglidis, and J. Dobaczewski, *Phys. Rev. C* **70**, 024607 (2004), and references therein.
- [4] S. Karataglidis, P. J. Dortmans, K. Amos, and C. Bennhold, *Phys. Rev. C* **61**, 024319 (2000).
- [5] M. Sharma, A. Bhagwat, Z. A. Khan, W. Haider, and Y. K. Gambhir, *Phys. Rev. C* **83**, 031601(R) (2011).
- [6] A. A. Korshennikov *et al.*, *Nucl. Phys. A* **617**, 45 (1997).
- [7] T. Uesaka *et al.*, *Phys. Rev. C* **82**, 021602 (2010).
- [8] D. Pachouri, S. Rafi, W. Haider, *J. Phys. G* **39**, 055101 (2012).
- [9] W. Haider, A. M. Kobos, and J. R. Rook, *Nucl. Phys. A* **480**, 20 (1988).
- [10] S. M. Saliem and W. Haider, *J. Phys. G* **28**, 1313 (2002).
- [11] I. E. Lagris and V. R. Pandharipande, *Nucl. Phys. A* **359**, 331 (1981).
- [12] R. B. Wiringa, V. G. J. Stoks, and R. Schiavilla, *Phys. Rev. C* **51**, 38 (1995).
- [13] V. G. J. Stoks, R. A. M. Klomp, C. P. F. Terheggen, and J. J. de Swart, *Phys. Rev. C* **49**, 2950 (1994).
- [14] K. A. Brueckner, J. L. Gammel, and H. Weitzner, *Phys. Rev.* **110**, 431 (1956).
- [15] J. W. Negele, *Phys. Rev. C* **1**, 1260 (1970).
- [16] F. A. Brieva and J. R. Rook, *Nucl. Phys. A* **297**, 206 (1978).
- [17] R. S. Mackintosh and N. Keeley, *Phys. Rev. C* **81**, 034612 (2010).
- [18] W. Haider, A. M. Kobos, and J. R. Rook, *Nucl. Phys. A* **480**, 1 (1988).
- [19] N. Yamaguchi, S. Nagata, and J. Matsuda, *Prog. Theor. Phys.* **70**, 459 (1983).
- [20] T. Furumoto, Y. Sakuragi, and Y. Yamamoto, *Phys. Rev. C* **78**, 044610 (2008).
- [21] A. Bhagwat, Y. K. Gambhir, and S. H. Patil, *Eur. Phys. J. A* **8**, 511 (2000); *J. Phys. G* **27**, B1 (2001), and references therein.
- [22] Y. K. Gambhir and S. H. Patil, *Z. Phys. A* **321**, 161 (1985); **324**, 9 (1986).
- [23] I. N. Boboshin *et al.*, *Bull. Russ. Acad. Sci.: Phys.* **73**, 810 (2009). The database of the Lomonosov Moscow State University, Skobeltsyn Institute of Nuclear Physics, is accessible at <http://cdfc.sinp.msu.ru/services/radchart/radmain.html>. The charge radii used in the present work are the recommended values by I. Angeli (see <http://cdfc.sinp.msu.ru/services/radchart/radhelp.html#rad>).
- [24] J. S. Al-Khalili, J. A. Tostevin, and I. J. Thompson, *Phys. Rev. C* **54**, 1843 (1996).
- [25] J. A. Tostevin and J. S. Al-Khalili, *Nucl. Phys. A* **616**, 418c (1997).
- [26] R. Sanchez *et al.*, *Phys. Rev. Lett.* **96**, 033002 (2006).
- [27] R. Sanchez *et al.*, *Hyperfine Interact.* **171**, 181 (2006).
- [28] G. Ewald *et al.*, *Phys. Rev. Lett.* **93**, 113002 (2004).
- [29] P. Mueller *et al.*, *Phys. Rev. Lett.* **99**, 252501 (2007).
- [30] H. De Vries, C. W. De Jager, and C. De Vries, *At. Data Nucl. Data Tables* **36**, 495 (1987).
- [31] J. S. McCarthy, I. Sick, and R. R. Whitney, *Phys. Rev. C* **15**, 1396 (1977).
- [32] D. Aleksandrov *et al.*, *Nucl. Phys. A* **633**, 234 (1998).
- [33] B. S. Pudliner, V. R. Pandharipande, J. Carlson, and R. B. Wiringa, *Phys. Rev. Lett.* **74**, 4396 (1995).
- [34] J. Wurzer and H. M. Hofmann, *Phys. Rev. C* **55**, 688 (1997).
- [35] A. Csoto, *Phys. Rev. C* **48**, 165 (1993).
- [36] W. Glockle and H. Kamada, *Phys. Rev. Lett.* **71**, 971 (1993).
- [37] A. Kievsky, M. V. Viani, and S. Roseti, *Nucl. Phys. A* **551**, 841 (1993); **577**, 511 (1994).
- [38] S. Burzynski, J. Campbell, M. Hammans, R. Henneck, W. Lorenzon, M. A. Pickar, and I. Sick, *Phys. Rev. C* **39**, 56 (1989).
- [39] M. V. Zhukov *et al.*, *Phys. Rep.* **231**, 151 (1993).
- [40] R. Henneck *et al.*, *Nucl. Phys. A* **571**, 541 (1994).
- [41] F. Petrovich *et al.*, *Nucl. Phys. A* **563**, 387 (1993).
- [42] C.-B. Moon *et al.*, *Phys. Lett. B* **297**, 39 (1992).